INTERPHASE TAILORING IN MULTIFUNCTIONAL GLASS/EPOXY COMPOSITES BY GRAPHENE OXIDE AND REDUCED GRAPHENE OXIDE

Haroon Mahmood and Alessandro Pegoretti

Department of Industrial Engineering, University of Trento, via Sommarive 9 – 38123 Trento – Italy
Email: haroon.mahmood@unitn.it, alessandro.pegoretti@unitn.it, Website: www.unitn.it

Keywords: Graphene, Fiber reinforced polymer composites, Interphase, Multifunctional properties, Electrophoretic deposition

ABSTRACT

Multiscale glass/epoxy composites were created by electrophoretic deposition (EPD) of graphene oxide (GO) nanosheets on glass fibers (GF). Modified Hummer's method and subsequent ultrasonication technique was used to create GO suspension from graphite source. A stable suspension of GO was used as a bath for EPD process where, being GO negatively charged, GF were placed in front of a metallic anode for an uniform GO coating. The deposition was carried out under various applied electric deposition fields (up to 10 V/cm) for a fixed amount of time (5 min). SEM observations (Fig. 1) confirm a fairly uniform coating of GO over the fiber surface. rGO coated fibers were also obtained by exposure of the GO coated fibers in an atmosphere of hydrazine hydrate at elevated temperature (100°C) which reduced the GO coating. XPS analysis was used to determine the level of reduction which confirmed the lowering of oxygen content in the coatings from 34% of GO to 10% of rGO. Both GO and rGO coated fibers were used to create hierarchical composites using an epoxy matrix.

The influence of the presence of a GO or rGO interphase on the mechanical behaviour of glass/epoxy composites was evaluated by various experimental techniques. By the single fiber fragmentation test an improved interfacial adhesion (ISS) was observed for both GO and rGO based composites compared to uncoated fiber. It is worthwhile to note that GO coating resulted to be more effective in enhancing the ISS values owing to the presence of a higher amount of functional groups, as indicated by FTIR analysis. Friction force microscopy was applied on the GO coated fibers which revealed a better coating/substrate adhesion confirming the interfacial reinforcement by graphene interphase. Flexural and interlaminar mechanical properties were also improved for both GO and rGO based macrocomposites.

Multifunctionality in the rGO based composites was also tested. Electrical and thermal conductivity of the composites not only revealed the influence of rGO as an 'active' nanofiller in the composite but also the advantage of unidirectional alignment of rGO coated fibers showed an increased level of conductivity in the longitudinal direction of composites as compared to transversal and vertical directions. The rGO coated fibers revealed an increased permittivity as compared to GO and uncoated fiber based composites not only confirming the dielectric properties but also giving a possibility of using such materials for shielding from electromagnetic radiations. The work confirms the possibility of graphene interphase in fiber/polymer composites not only improving mechanical properties but also inducing multifunctionality in the structures (Fig. 2).

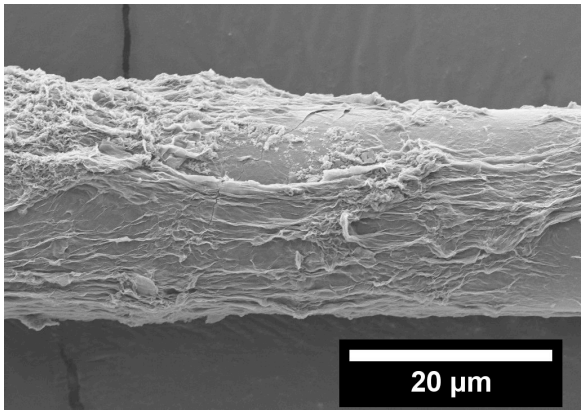

Fig. 1 Scanning electron microscopy image of GF coated with GO.

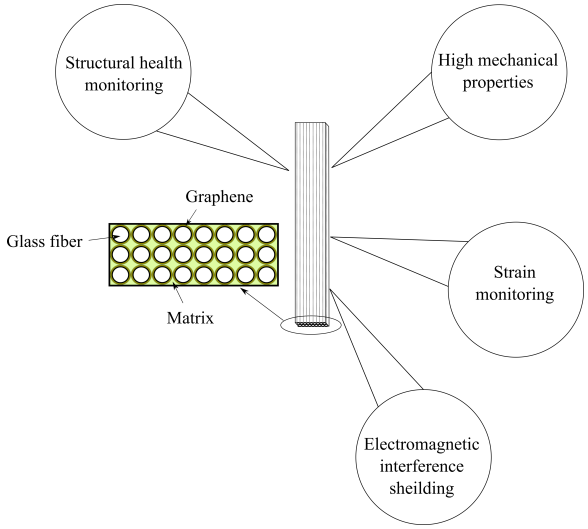

Fig 2. Graphene coated fibers reinforced in polymer matrix – Opportunities in engineering applications.

1 INTRODUCTION

Fiber-reinforced polymer composites are widely used in recent days in many engineering applications like advance aerospace systems, automobile sectors, wind turbines, civil structures, etc. This is due to the advantages composite materials can provide, such as high strength-to-weight ratio, high impact resistance, corrosion resistance and easy assembly of complex components.

The properties of fiber-reinforced composites mainly depend on the interfacial adhesion between the matrix and the fiber. In fact, a better interfacial adhesion would result in better load transfer from the matrix to the fiber, hence the load bearing capacity of the composite increases with the improvement in the fiber/matrix adhesion. This adhesion could be determined by mechanical interlocking or by chemical and physical interactions. [1] . The improvement of interlocking phenomena can be approached via various methods like interphase tailoring, nanostructure based hierarchical fibers, polymer deposited fiber surface modification and matrix modification for better interphase formation [2] . The most challenging method in this field is the development of hierarchical micro/nano composites that has been utilized with great interest to create nanoscale reinforcement on fibers.

The most promising nanoscale reinforcement used in such strategy is graphene due to its superlative properties like high electron mobility, record breaking strength and high Young's modulus [3-5] . Various research groups have reported the positive effect obtained by incorporating graphene in polymer based materials like better mechanical properties [6-9] . The basis on interaction

between the polymer and graphene nanosheets are either weak van der Waal's forces and π-π stacking. Oxidized form of graphene has proven to give better interactions in polymer matrices due to the presence of polar functionalities based on oxygen-containing groups [10] .

Improvement in composite properties has been possible even at a very low nanofiller content which is a consequence of the extremely large surface area of the nanofiller along with its high aspect ratio. However, the improvement in the properties reached until now is not many folds as predicted by theoretical calculations due to some practical issues like uniform dispersion of nanofiller, near to perfect interfacial adhesion between matrix and nanofiller and alignment of nanofillers. In the past, various techniques have been employed like mechanical mixing at high energy, application of both electrical and magnetic fields [11, 12] during the fabrication process of composites in order to achieve better dispersion and alignment of the nanofiller but there has been far little improvement than expected .

Starting from the above considerations, this work shows the possibility to align graphene nanosheets in the composites by their selective deposition at the fiber/matrix interface region. In particular, electrophoretic deposition (EPD) is utilized to coat the glass fibers (GF) to reach a uniform coating of well aligned graphene-based nanosheets (graphene oxide or reduced graphene oxide). Epoxy-based composites prepared with GO or rGO coated GF were tested to investigate changes in the mechanical properties caused by the graphene based interphase. Moreover, the possibility of having electrically and thermally conductive composites due to the presence of a rGO interphase in epoxy/glass composites was experimentally investigated.

2 MATERIALS AND METHODS

Graphite powder, potassium permanganate, sodium nitrate, sulfuric acid and hydrogen peroxide were purchased from Sigma Aldrich while hydrochloric acid was provided by Codec Chemical Co. Ltd. A bi-component epoxy resin, provided by Elantas Italia S.r.l. (Collecchio, Italy), consisting of a resin (EC 252) and a hardner (W 241), was selected as polymer matrix. All chemicals were of analytical grade and used without further purification. E-glass fibers, with the trade code XG 2089, were kindly supplied by PPG Fiber Glass and used as received. These had an average diameter of 16.0 ± 0.1 μm with an epoxy compatible sizing.

GO was synthesized according to a modified version of the Hummer's method [13] . Briefly, 1 g of graphite powder was mixed in 46 ml of H_2SO_4 cooled in an ice bath. 1 g of $NaNO_3$ was added later on and the mixture was stirred for 15 min. Later, 6 g of $KMnO_4$ was slowly added while keeping the mixture's temperature under 20°C in order to avoid exothermic reactions. The mixture was then stirred for at least 24 h at 35° C. Then, a deionized water in large quantity was added to the mixture prepared while the temperature was kept between 60° to 80° C. At the end, a solution of 30% H_2O_2 with deionized water was added to the mixture to stop the reaction. The resulting suspension was thoroughly washed using a HCl solution and distilled water to remove Mn ions and acid respectively. The obtained brown solution was dried in a vacuum oven at 50° C for at least 36 h. The brown cake obtained was then used to create GO suspension (1 mg/ml) by adding a quantity of it in deionized water and subjecting it to ultrasonication to create a stable suspension.

A schematic description of the EPD process used to deposit GO nanosheets on GFs is illustrated in Figure 3. Copper sheets of 1 mm thickness were used as electrodes and GF were placed in front of the anode using a metallic window. This approach is needed due to the non-conducting nature of GF. Therefore, in order to deposit the nanoparticles on the GF, anode was placed behind the fibers during the deposition process. The electrodes along with metallic frame containing GF were immersed in a water GO dispersion of 1 mg/ml concentration. When voltage was applied between the electrodes, GO nanosheets were force to move toward the anode, hit GFs and deposited on their surface. The deposition on one side of the fibers was carried out at 10V/cm for 5 min and the same was repeated while reversing the metallic frame to expose the uncoated portion towards cathode while coated side of the fibers towards the anode. After the whole coating process, the fibers were dried under vacuum at 50°C for at least 12 h.

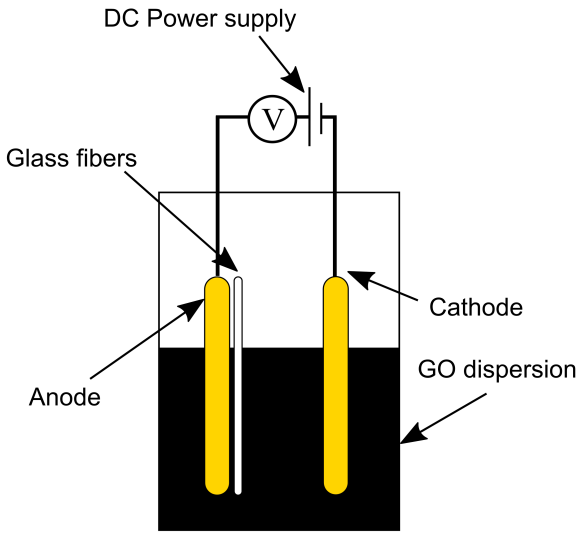

Figure 3: Schematic diagram of electrophoretic deposition (EPD) of graphene oxide (GO) on glass fibers (GF).

Reduction of GO coated GF was performed by placing the fibers in a suitable glass container and placing a tissue paper soaked with hydrazine hydrate (N_2H_4) in the container. The container was covered and heated at 100°C for 24h to reduce the GO coating on the fibers.

A conventional hand lay-up method was used to fabricate unidirectional composites. The uncoated GF, GO coated GF and rGO coated GF (in the form of laminates) were stacked while resin was infused within the fibers using a roller. After laminating a number of laminas enough to reach the desired laminate thickness (which in turns depends on the type of test performed), a constant pressure of approximately 10 kPa was applied on the mold and curing was performed by pre-curing at room temperature for at least 3 hours and then for 15 hours at 60°C. The obtained composites with neat GF fibers, GF fibers coated with GO or rGO were termed as Ep-GF, Ep-GO-GF and Ep-rGO-GF, respectively.

3 CHARACTERIZATION AND TESTING

X-ray diffraction (XRD) measurements were performed with a X-ray diffractometer (Rigaku III D-max) with a monochromatic radiation source of Cu-Kα line of wavelength around 51.54056 Å in the 2θ range of 5-80° with a step size of 0.04°. Fourier transform infrared (FTIR) spectroscopic measurements were recorded using a Nikolet Avatar 330 device with a 4 cm^{-1} resolution. The samples were prepared by mixing the samples in tiny amount with KBr powder and forming thin discs in a mold under a compressive pressure of 10 bar. X-ray photoelectron spectroscopy (XPS) analysis was executed by utilizing a Kratos Axis Ultra DLD machine fitted with a hemispherical analyzer and a monochromatic Al Kα (1486.6 eV) x-ray source. A 90° emission angle between the axis of the analyzer and the sample surface was adjusted. O 1s and C 1s core lines of each sample were collected while the quantification, described as relative elemental percentage, was achieved using the integrated area of the fitted core lines, after Shirley background subtraction, and correcting for the instrument sensitivity factors. Field emission scanning electron microscopy (FESEM) microscopic images were taken by a Zeiss Supra 40 microscope (Berlin, Germany). The specimens were coated by a platinum/palladium alloy (80:20) thin coating of about 5 nm.

Friction force microscopy (FFM) was performed in contact mode through an atomic force microscopy (AFM) model DCP01_NTMDT using diamond coated cantilever tip apex [9] .
Here, AFM plays a dual role of mapping and manipulating the substrate in a sequential manner. Sader method [14, 15] was applied to measure normal (K_N) and torsional (K_T) spring constants of cantilever. Typical values of $K_N = 6.03\times10^8$ N/m and $K_T = 8.25\times10^8$ N/m for cantilever with tip radius of 51 nm were obtained. Calibrated tip was slid from bare GF to GO covered region at a fixed normal force (F_N)

[9] .

The cross-section of multiscale composites was observed by optical microscopy technique (using a Zeiss Axiophot optical microscope, connected to a Leica DC300 digital camera) and by FESEM. The specimens were prepared by polishing the cross-sectional surface using abrasive grinding papers with grit size 800, 1200 and 4000 sequentially.

Three-point bending tests were performed according to ASTM D790 on specimens with dimensions of around 80 mm × 13 mm × 1 mm, while the span to depth ratio was fixed at 60:1 and 40:1 for determining flexural modulus and flexural strength, respectively. An Instron 5969 electromechanical testing machine equipped with a 50 kN load cell was used for this purpose. Therefore, in order to maintain a strain rate of 0.01 mm^{-1}, a cross-head speed of 6.9 mm/min for flexural modulus evaluation and 3.1 mm/min for flexural strength evaluation was respectively adopted. Short beam shear test were performed using Instron 5969 electromechanical testing machine equipped with a 50 kN load cell to evaluate an interlaminar shear strength of the laminates according to ASTM D2344 standard. At least 5 specimens of 4 mm thickness were tested under 3 point bending conditions at a cross-head speed of 1 mm/min until the deflection equal to the thickness of the sample was achieved. The maximum corresponding force (F_m) value was used to evaluate the interlaminar shear strength as:

$$ILSS = 0.75 \times \frac{F_m}{b \times h} \tag{1}$$

Mode I fracture toughness tests were performed according to the standard ASTM D5528. Composite specimens were fabricated with 18 laminae and a middle crack starter constituted by a thin (thickness = 23 μm) Teflon film insert. The final dimensions of the specimen were around 180 mm × 25 mm × 4 mm. To load the sample under opening mode I, piano hinges were attached. A digital webcam (Logitech B910 HD) was used to record crack advancement simultaneously with the applied load. Tests were performed at a cross-head speed of 2.5 mm/min on at least 3 specimens for each sample and the results were analyzed by considering three different criteria: i) deviation from linearity (NL) point obtained by considering the point in load-displacement plots where deviation from linearity is observed; ii) visual observation (VIS) point where the delamination was visually observed to grow from the insert; iii) maximum load (MAX) point represented by the highest load measured during the test as obtained from the load-displacement plot.

To measure the electrical resistivity of the samples, two different methods were used depending on the electrical behaviour of the composites. Specimens presenting high resistivity levels (>10^6 Ωcm), were tested using a Keithley 8009 resistivity test chamber connected to a Keithley 6517A high-resistance meter. On the other hand, more conductive samples were tested via a 6-1/2-digit electrometer/high resistance system (Keithley model 6517A) and 2-points electrical measurement was chosen as test configuration. Moreover, the effect of a continuous interphase in conductive samples was also investigated by measuring the electrical conductivity along three orthogonal directions as defined in Figure 4.

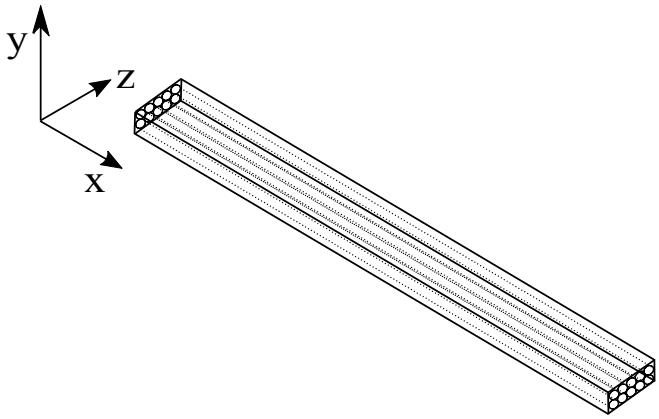

Figure 4: Description of directions in terms of orientation for electrical and thermal conductivities

measurements.

Relative permittivity and dielectric loss of the composites (uncoated and graphene reinforced composites) were measured using an Agilent 4284A impedance analyzer in the frequency range from 20 up to 10^6 Hz. Specimens with dimensions around 10 mm × 10 mm × 1.5 mm were tested and an aluminum foil was used as conductive electrode plate placed on the two sides of the specimen to create the parallel plate testing configuration.

The advantage of a having continuous graphene based interphase along the fiber length was evaluated in the case of thermal conductivity measurements. Considering the directions of composites defined in Figure 5, composite specimens containing fibers (uncoated, GO or rGO coated) oriented in the thickness direction were prepared which were designated as x-axis (Figure 5a). In case of other directions of the composites which did not contain a continuous interphase network of graphene, such sample types were prepared where the fibers were oriented along the length of the specimen termed as y-axis and z-axis (Figure 5b).

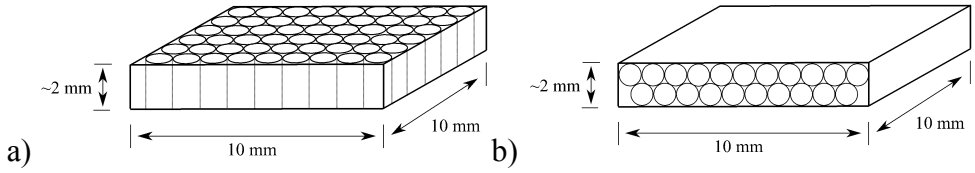

Figure 5: Schematic diagram of composite sample with fibers a) through the thickness direction (x-axis), b) along the in plane directions (y-axis and z-axis)

Thermal conductivity measurements were performed by a Netzsch Laser Flash Analysis LFA 447. The test consists in exposing one side of a specimen (10mm × 10mm × 2mm) to an energy pulse from a light source (laser or xenon flash lamp) and measuring the temperature history on the other side by a liquid nitrogen cooled infrared detector. The thermal conductivity of the specimens was measured at 25°C performing 3 shots along x-, y- and z-axis. The data was analyzed using the software Proteus whereas Cowan method was used to calculate thermal diffusivity (α) along with the pulse correction. A standard Pyrex 7740 reference material prepared according to ASTM-E 1461 was used to determine the heat capacity (c_p) and was matched with the samples. Sample density (ρ) was determined by measuring the mass and volume of the specimen. Finally, the thermal conductivity (λ) was calculated using the following equation:

$$\lambda = \alpha \times \rho \times c_p \tag{2}$$

4 RESULTS AND DISCUSSIONS

The X-ray diffractograms of precursor graphite, synthesized GO and rGO products are presented in Figure 6a. Graphite exhibits a characteristic peak (002) at 26.4° while its chemical reaction during graphene synthesis replaced the (002) peak with the (001) diffraction peak of GO. This is due to the addition of oxygen based functional groups and water molecules in GO resulting in the increase of the interlayer spacing in the graphite layers [16] . On the other hand, rGO diffractogram revealed the same peak relocated back to the position of pristine graphite peak due to the removal of most of the oxygen groups of GO and the consequent lowering of the interlayer spacing. The FTIR spectra of graphite, GO and rGO are compared in Figure 6b. GO showed relatively intense peaks at wavenumbers 3830 cm^{-1}, 1625 cm^{-1} and 1085 cm^{-1} as compared to pristine graphite (associated to groups like O-H, C=O and C-O respectively) which derive from the destruction of extended conjugated π-orbital system and insertion of oxygen-containing functional groups into carbon skeleton. The chemical reduction with hydrazine hydrate lowered the intensity of the functional groups peaks of rGO spectra. Figure 6c displays the surface chemical composition of GO and rGO samples as determined by XPS analysis. The C1s XPS spectrum of GO reveals a particular degree of oxidation

with some functional groups namely the carboxyl group (COOH), the C in C-O bonds and non-oxygenated carbon (C-C) attached to the carbon skeleton. Using the atomic sensitivity factors, the oxygen and carbon content in GO resulted to be of 34% and 66%, respectively. The XPS spectrum of rGO also confirmed the existence of the same oxygenated functional groups but with a reduced intensity of the peaks. In addition, since the chemical reduction of GO occurred in the nitrogen-rich environment of hydrazine hydrate, a new C-N group is visible in rGO spectrum. The percentages of oxygen and carbon of rGO specimen resulted to be of 10% and 90%, respectively. The characteristic wrinkling of nanosheets as observed from FESEM picture reported in Figure 6d provides indications about the exfoliation of GO sheets. The nanosheets display a lateral size of several micrometers but with few layers thickness.

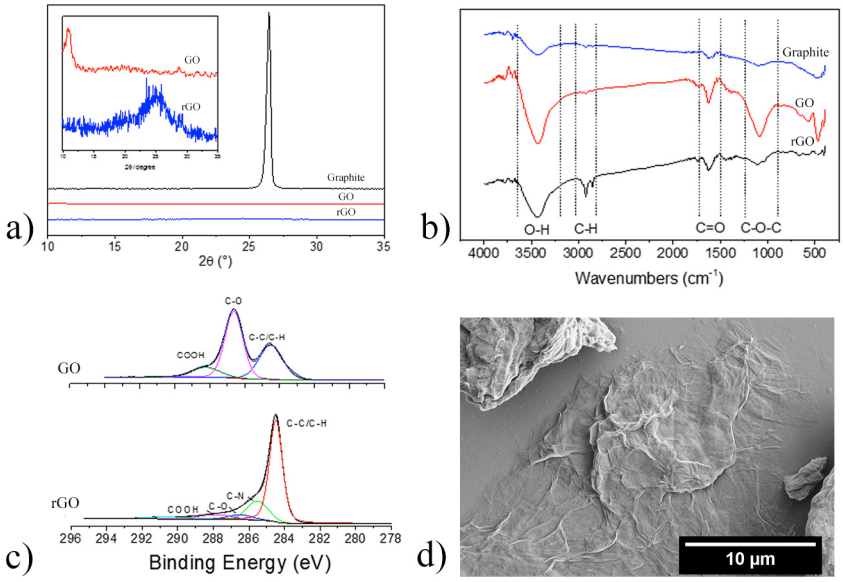

Figure 6. Results of a) X-ray diffraction, b) Fourier transform infrared spectroscopy, c) XPS and d) FESEM analysis.

The electrophoretic deposition of GO and rGO on GF could be visualized using FESEM observations. In Figure 7, a comparison of the uncoated, GO and rGO coated GF surfaces is presented where the coating of both GO and rGO at a certain length appears to be quite uniform in thickness.

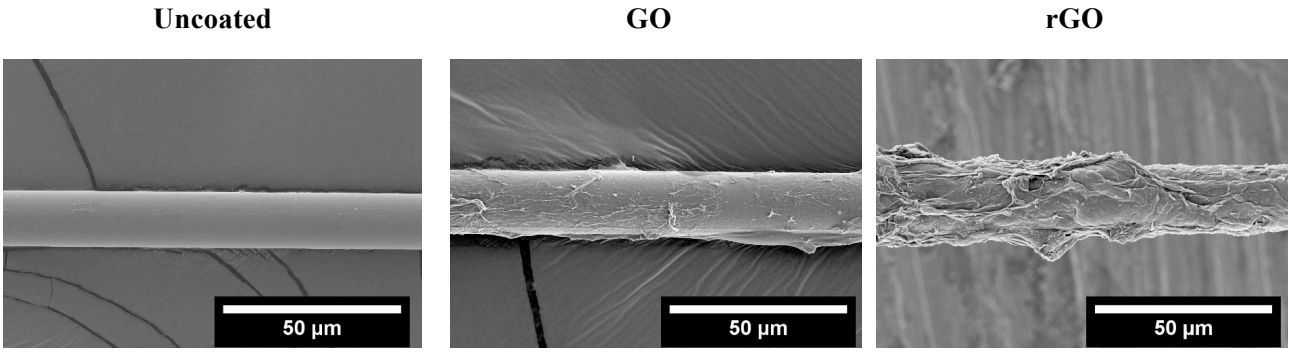

Figure 7. FESEM pictures of uncoated, GO coated and rGO coated GF.

The fiber volume fraction of the composites was determined quantitatively by considering the weight of the fibers before composite fabrication and then measuring the weight of the whole

composite after curing. The weight of the matrix was then calculated by subtracting the weight of the composite from the weight of the fiber and by considering the densities of the fiber and the matrix, the fiber volume fraction was estimated to be about 50 %, whereas the amount of graphene coating was around 0.3%.

The typical flexural stress-strain curve and the resulting flexural modulus and strength of the composites are reported in Figure 8. Both GO and rGO coating reinforced the composites thus enabling them to bear higher loads as compared to uncoated fibers. The flexural modulus increased by 19% and 9% for GO and rGO coated GF, respectively, as compared to composites with uncoated fibers. The flexural strength of the composites containing GO showed an increase by 20%. The increase in strength is related to the fact that GO interphase between the matrix and the fibers improved the bonding level and mechanical interlocking phenomena [9]. Nevertheless, in case of rGO, the strength is practically the same as compared to composites with uncoated fibers. This fact could be attributed to the weak interfacial adhesion between rGO and epoxy matrix.

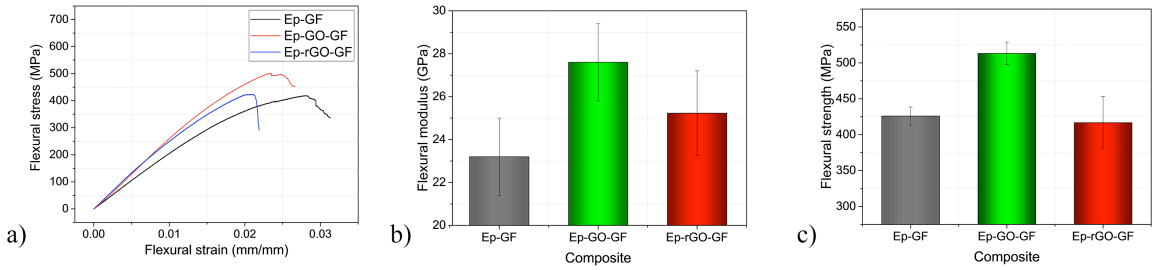

Figure 8. Flexural tests data of composites: a) stress- strain curves b) flexural modulus and b) flexural strength.

The interlaminar shear strength (ILSS) of the composites was investigated by the short beam shear test and the obtained load-displacement curves are reported in Figure 9a. A positive effect of GO interphase in epoxy/glass composites is documented in the 15% increase of ILSS values as compared to composites with uncoated fibers. At the same time, a 9% increase was found for rGO based glass/epoxy composites (Figure 9b). This result confirmed our previous observations in which GO coated fibers offered both a better chemical interaction with the epoxy matrix, due oxygen-based functional groups, and mechanical interlocking [9]. This better load transfer via the interface resulted in an enhancement in interfacial strength finally translated into higher ILSS values. In case of epoxy composites reinforced with rGO coated glass fibers the main reinforcing mechanism is the mechanical interlocking which leaded to an increase of ILSS values but not as high as for GO-coated fibers due to the lower amount of oxygen-based functional groups on the surface of rGO.

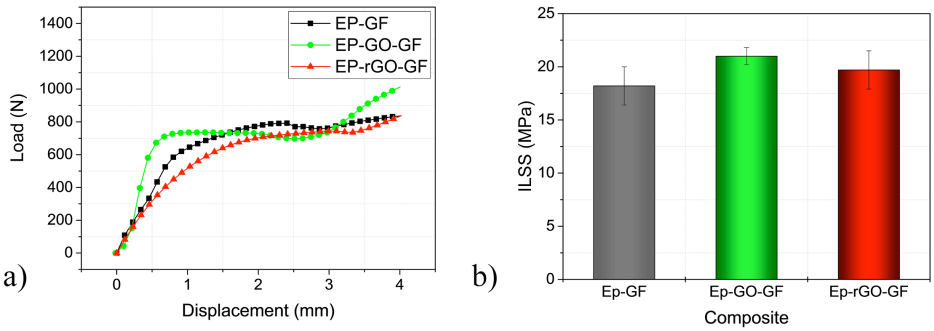

Figure 9. Interlaminar shear strength as determined by short beam strength test where a) represents the typical load-displacement curves of composites while b) shows the comparison of ILSS values.

In case of Mode I fracture toughness tests, the critical strain energies values were evaluated from the load-displacement plot of Figure 10a and plotted as resistance curves (R-curves) as shown in

Figure 10b. Table 1 shows the average values of the three composites tested. As it can be seen, composite reinforced with GO coated GF showed an increment of the NL and VIS G_{Ic} values as compared to composites with rGO coated GF and uncoated GF. The G_{Ic} values computed according to the MAX procedure are however practically the same for all the investigated composites. rGO coated GF fibers also provided some resistance to crack propagation but not at the level of composites with GO coated fibers. This investigation clearly shows the higher energy required for crack propagation when GO was deposited on GF as a continuous reinforcing interphase in epoxy/glass composites.

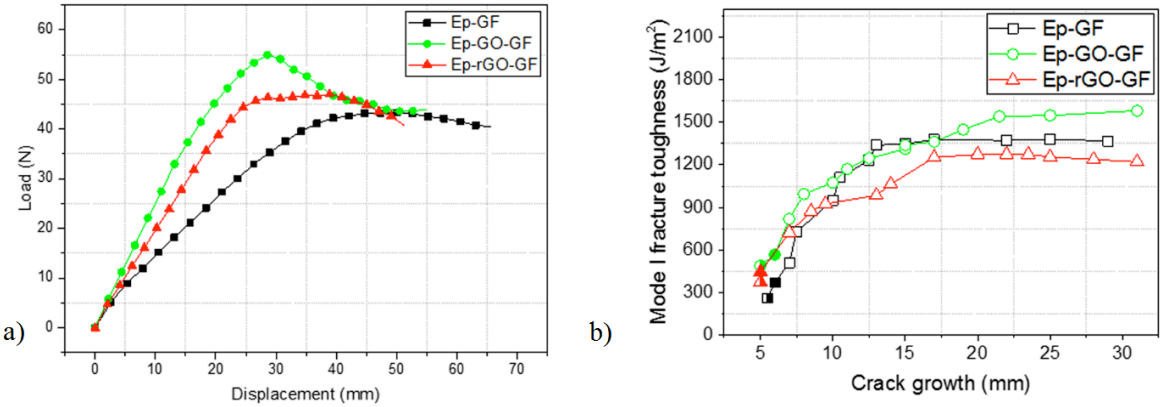

Figure 10. Typical load-displacement curves of DCB specimens loaded under Mode I and corresponding fracture toughness R-curves.

Specimen	Nonlinearity (NL)	Visual observation (VIS)	Maximum load (MAX)
	(J/m^2)	(J/m^2)	(J/m^2)
Ep-GF	243.5 ± 21.5	401.8 ± 46.3	1176.4 ± 244.9
Ep-GO-GF	384.3 ± 92.6	692.9 ± 145.1	1275.8 ± 180.5
Ep-rGO-GF	352.8 ± 27.0	407.9 ± 52.8	1153.2 ± 141.7

Table 1. Mode I fracture toughness (G_{Ic}) values of Ep-GF, Ep-GO-GF and Ep-rGO-GF composites.

All composites were subjected to electrical resistivity measurement and the main results are summarized in Figure 11a. Due to the insulating nature of both epoxy matrix and GF, composite with uncoated GF presented high resistivity values (around 10^{14} Ω cm). Unsurprisingly, the presence of a GO interphase in Ep-GO-GF also did not modify the electrical behaviour and a resistivity value around 10^{13} Ω cm was obtained. This is in accordance to the fact that GO nanosheets are insulating in nature due to the presence of substantial electronic disorder arising from variable sp^2 and sp^3 bonds. However, in case of Ep-rGO-GF composites, the presence of a conductive rGO coating on GF gave the entire system a conductive nature with resistivity values lower than 10^2 Ω cm. This result confirms the successful reduction of GO to rGO [17] . In order to investigate any possible anisotropy in the electrical behaviour of having a continuous interphase oriented along the fibers direction, the electrical resistivity of the conductive composite was tested along three mutually orthogonal directions i.e. x-axis, y-axis and z-axis. In Figure 11b, the volume resistivity values along the three directions of rGO based composite are compared. The composites showed a very low resistivity along the x-axis which contains the continuous path for electrons to travel through the structure. On the other hand, the y-axis and z-axis showed higher resistivity values because of the alternating conductive (graphene) and non-conductive (epoxy) layers. Moreover, y-axis manifests lower resistivity as compared to z-axis as the pressure was applied along this direction during the composite manufacturing thus compressing the fibers and providing better contacts between them.

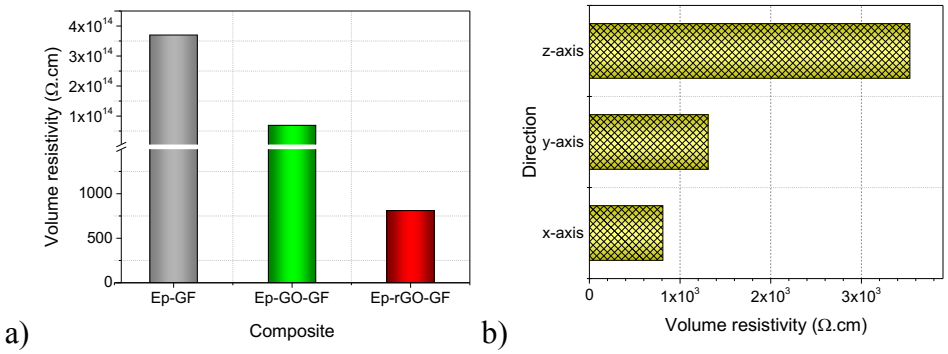

Figure 11. a) Volume resistivity of Ep-GF, Ep-GO-GF and Ep-rGO-GF composites, b) Volume resistivity of Ep-rGO-GF composites measured along three different directions of the sample with respect to fiber orientation [IOP Conference Series: Materials Science and Engineering 139(1) (2016) 012004].

The permittivity of composite with uncoated fiber was measured at room temperature as a control test. As reported in Figure 12, the permittivity level did not change as the applied frequency increased, which is in accordance with the behavior commonly observed for insulating materials such as neat epoxy and GF. Composites based on GO-coated GF also did not display any capacitive response due to its electrically insulating behavior. In the case of rGO-coated fibers, however, the composite showed a strong improvement of the dielectric constant over the entire frequency range. At 100 Hz the permittivity value increased by a factor of 3.6 when compared to the value measured on the composite with uncoated fibers. The induction of permittivity in glass/epoxy composites was due to the presence of rGO interphase which possesses a higher electrical conductivity.

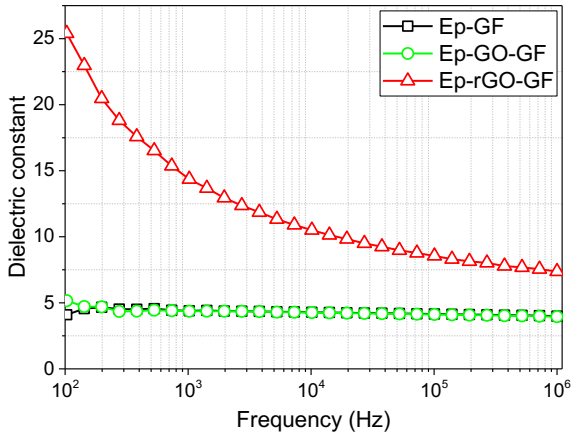

Figure 12. Permittivity of composites (EP-GF, Ep-GO-GF and Ep-rGO-GF).

The thermal conductivity of the samples was tested at 25°C along three different mutual orthogonal directions (x-, y- and z-axis) and the results are summarized in Figure 13. It is interesting to observe that the thermal conductivity of composites containing GO and rGO coated fibers was significantly higher that that of composites with uncoated fibers. Moreover, as expected, the thermal conductivity values of composites with rGO coated fibers were higher than that prepared with GO coated fibers. This increase in conductivity was induced by the higher thermal conductivity of rGO as compared to GO nanosheets which again confirms the successful reduction of GO during chemical treatment with hydrazine hydrate. This also shows the advantage of aligning the nanosheets as a continuous interphase between the matrix and fiber, even with a very low content of rGO nanosheets, which improved the thermal conductivity by 20% as compared to neat composites (without any interphase). Along the y- and z-axis of the composites the thermal conductivity did not show any significant change as reported in Figure 13. This was due to the very low content of GO or rGO nanosheets along

these two directions which makes it impossible to create a percolation threshold enough to improve the thermal conductivity as like in the x-direction (along the fiber) which presents a continuous interphase.

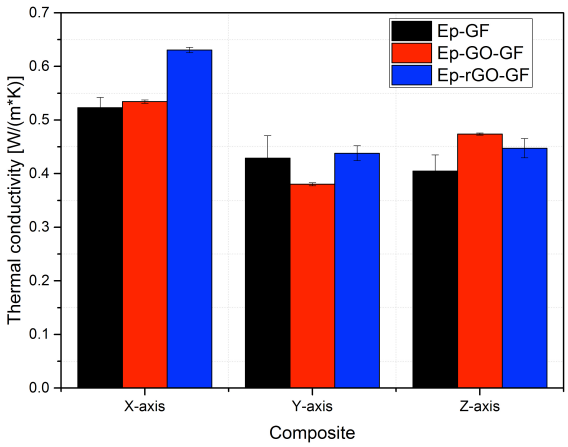

Figure 13. Thermal conductivity of composites at 25°C along different orientations.

5 CONCLUSIONS

It was seen that epoxy/glass composites with GO interphase possessed enhanced flexural modulus and flexural strength while those with rGO-coated fibers showed minor improvement in flexural properties. Short-beam shear (SBS) tests provided similar information. In fact, composites based on GO-coated fibers showed an increased interlaminar shear strength while for those prepared with rGO-coated fibers only slightly improvement of interlaminar shear strength was observed. Mode I fracture toughness tests on the composites confirmed the positive influence on the interlaminar adhesion exerted by the presence of a GO interphase. On the other hand, rGO based epoxy/glass composites manifested a slightly reduced toughness under opening loading mode.

Electrical resistivity measurements indicated that rGO based epoxy/glass composites presents a reduced resistivity due to the conductive nature of rGO nanosheets, whereas there was no difference between the composites based on uncoated and GO coated fibers (which showed insulating behavior). An in-depth analysis revealed that the directional orientation or rGO nanosheets along the length of the fibers offered the lowest resistivity as compared to other orientations hence confirming the advantage of oriented and aligned rGO interphase for tailored functional properties. The conductive behavior of epoxy/glass composite containing rGO interphase also induced permittivity in the composites. This was confirmed along with the other composites containing uncoated and GO coated fibers. This functionality proposes the possibility to use such composites for electromagnetic interference shielding in advanced applications. Other than electrical functionalities, aligned rGO interphase along with the fibers in epoxy/glass composites offered better thermal conductivity. This was confirmed by comparing the thermal conductivity values along different orientations in the composites based on either uncoated, GO or rGO coated GF. This result supports the advantage of aligning graphene interphase in epoxy/glass composites for improved functional properties.

ACKNOWLEDGEMENTS

The valuable support provided by dr. S.H. Unterberger of the Unit for Material Technology, University of Innsbruck, Austria, for the thermal conductivity measurements is kindly acknowledged.

REFERENCES

[1] F.R. Jones, A Review of Interphase Formation and Design in Fibre-Reinforced Composites, Journal of Adhesion Science and Technology 24, 2010, pp. 171-202 (doi: 10.1163/016942409X12579497420609)

[2] J. Karger-Kocsis, H. Mahmood, A. Pegoretti, Recent advances in fiber/matrix interphase engineering for polymer composites, Progress in Materials Science 73, 2015, pp. 1-43 (doi: 10.1016/j.pmatsci.2015.02.003)

[3] K.S. Novoselov, A.K. Geim, S.V. Morozov, D. Jiang, Y. Zhang, S.V. Dubonos, I.V. Grigorieva, A.A. Firsov, Electric field effect in atomically thin carbon films, Science 306, 2004, pp. 666-9 (doi: 10.1126/science.1102896)

[4] C. Lee, X. Wei, J.W. Kysar, J. Hone, Measurement of the Elastic Properties and Intrinsic Strength of Monolayer Graphene, Science 321, 2008, pp. 385-388 (doi: 10.1126/science.1157996)

[5] A.A. Balandin, S. Ghosh, W. Bao, I. Calizo, D. Teweldebrhan, F. Miao, C.N. Lau, Superior Thermal Conductivity of Single-Layer Graphene, Nano Letters 8, 2008, pp. 902-907 (doi: 10.1021/nl0731872)

[6] D. Pedrazzoli, A. Pegoretti, Hybridization of short glass fiber polypropylene composites with nanosilica and graphite nanoplatelets, Journal of Reinforced Plastics and Composites 33, 2014, pp. 1682-1695 (doi: 10.1177/0731684414542668)

[7] D. Pedrazzoli, A. Pegoretti, Expanded graphite nanoplatelets as coupling agents in glass fiber reinforced polypropylene composites, Composites Part A: Applied Science and Manufacturing 66, 2014, pp. 25-34 (doi: 10.1016/j.compositesa.2014.06.016)

[8] D. Pedrazzoli, A. Pegoretti, K. Kalaitzidou, Understanding the effect of silica nanoparticles and exfoliated graphite nanoplatelets on the crystallization behavior of isotactic polypropylene, Polymer Engineering & Science 55, 2015, pp. 672-680 (doi: 10.1002/pen.23941)

[9] H. Mahmood, M. Tripathi, N. Pugno, A. Pegoretti, Enhancement of interfacial adhesion in glass fiber/epoxy composites by electrophoretic deposition of graphene oxide on glass fibers, Composites Science and Technology 126, 2016, pp. 149-157 (doi: 10.1016/j.compscitech.2016.02.016)

[10] Q. Cheng, M. Wu, M. Li, L. Jiang, Z. Tang, Ultratough Artificial Nacre Based on Conjugated Cross-linked Graphene Oxide, Angewandte Chemie 125, 2013, pp. 3838-3843 (doi: 10.1002/ange.201210166)

[11] J.G. Park, Q. Cheng, J. Lu, J. Bao, S. Li, Y. Tian, Z. Liang, C. Zhang, B. Wang, Thermal conductivity of MWCNT/epoxy composites: The effects of length, alignment and functionalization, Carbon 50, 2012, pp. 2083-2090 (doi: 10.1016/j.carbon.2011.12.046)

[12] M.-K. Schwarz, W. Bauhofer, K. Schulte, Alternating electric field induced agglomeration of carbon black filled resins, Polymer 43, 2002, pp. 3079-3082 (doi: 10.1016/S0032-3861(02)00084-8)

[13] W.S. Hummers, R.E. Offeman, Preparation of Graphitic Oxide, Journal of the American Chemical Society 80, 1958, pp. 1339-1339 (doi: 10.1021/ja01539a017)

[14] C.P. Green, H. Lioe, J.P. Cleveland, R. Proksch, P. Mulvaney, J.E. Sader, Normal and torsional spring constants of atomic force microscope cantilevers, Review of Scientific Instruments 75, 2004, pp. 1988-1996 (doi: 10.1063/1.1753100)

[15] J.E. Sader, J.W.M. Chon, P. Mulvaney, Calibration of rectangular atomic force microscope cantilevers, Review of Scientific Instruments 70, 1999, pp. 3967-3969 (doi: 10.1063/1.1150021)

[16] A. Buchsteiner, A. Lerf, J. Pieper, Water Dynamics in Graphite Oxide Investigated with Neutron Scattering, The Journal of Physical Chemistry B 110, 2006, pp. 22328-22338 (doi: 10.1021/jp0641132)

[17] A. Pegoretti, H. Mahmood, D. Pedrazzoli, K. Kalaitzidou, Improving fiber/matrix interfacial strength through graphene and graphene-oxide nano platelets, IOP Conference Series: Materials Science and Engineering 139, 2016, pp. 012004 (doi: 10.1088/1757-899X/139/1/012004)